Discover Oncology

RESEARCH Open Access

Identification of TRPM4 related genes in LUAD by RNA seq and spatial transcriptomics

Wei-jie Yu[1†], Zhou-lin Miao[2*†] and Julaiti Ainiwaer[3*]

†Zhou-lin Miao and Wei-jie Yu contributed equally to this work.

*Correspondence:
Zhou-lin Miao
442447335@qq.com
Julaiti Ainiwaer
13809901336@163.com
[1]Department of Thoracic Surgery, The Third Affiliated Hospital of Xinjiang Medical University, Urumuqi 839000, Xinjiang, China
[2]Radiology Department, University of Health and Rehabilitation Sciences (Qingdao Municipal Hospital), Qingdao 266000, Shandong, China
[3]Department of Thoracic Surgery, First Affffliated Hospital of Xinjiang Medical University/State Key Laboratory of Pathogenesis, Prevention and Treatment of High Incidence Diseases in Central Asia, Urumuqi 839000, Xinjiang, China

Abstract

Background Sodium overload-induced cell death is a novel mode of cell death that differs from other modes and is a very promising new target for cancer therapy. In addition, sodium overload-induced cell death plays a crucial role in cancer progression and patient prognosis. Therefore, our study aims to establish a survival prediction model for patients with lung adenocarcinoma (LUAD) based on related genes, exploring the immune landscape and providing new insights for future individualized treatment protocols.

Method We analyzed the expression and clinical significance of TRPM4-related genes in LUAD using data from TCGA and GEO databases. We used transcriptomics, immune infiltration assays, and spatial transcriptomics (ST). Kaplan-Meier survival analysis was used to assess the relationship between TRPM4-related genes and prognosis. Enrichment analyses identified biological processes and pathways associated with TRPM4 and also assessed its relationship with the immune microenvironment and drug sensitivity.

Results We identified 19 oncogenic driver genes and modeled proportional hazard regression. The results showed that the survival rate of the high-risk group was significantly reduced in both the training and testing sets. Additionally, the high-risk group exhibited lower levels of immune cell infiltration and immune checkpoint expression compared to the low-risk group. Based on 19 genes, LMNA, PPP2R1A, and PDXK were identified as key genes by single-cell sequencing and spatial transcriptome sequencing.

Keywords LUAD, Immune, TRPM4, Prognosis

1 Introduction

Lung cancer (LC) is the most common cancer globally and the top cause of cancer-related deaths [1]. Lung adenocarcinoma (LUAD), one of the major subtypes of non-small cell lung cancer (NSCLC), accounts for about 50% of all cases [1, 2]. The primary treatments for LC currently include surgery, chemotherapy, and targeted therapy. However, due to the disease's insidious onset, it is frequently diagnosed at an advanced stage. Many individuals lack access to surgical options. Unlike with other diseases, the 5-year survival rate for lung cancer has not seen significant improvement over the years, mainly

© The Author(s) 2026. **Open Access** This article is licensed under a Creative Commons Attribution-NonCommercial-NoDerivatives 4.0 International License, which permits any non-commercial use, sharing, distribution and reproduction in any medium or format, as long as you give appropriate credit to the original author(s) and the source, provide a link to the Creative Commons licence, and indicate if you modified the licensed material. You do not have permission under this licence to share adapted material derived from this article or parts of it. The images or other third party material in this article are included in the article's Creative Commons licence, unless indicated otherwise in a credit line to the material. If material is not included in the article's Creative Commons licence and your intended use is not permitted by statutory regulation or exceeds the permitted use, you will need to obtain permission directly from the copyright holder. To view a copy of this licence, visit http://creativecommons.org/licenses/by-nc-nd/4.0/.

due to the absence of effective biomarkers. Therapeutic approaches other than surgery may be hindered by the lack of effective gene targets, resulting in a 5-year survival rate that has not shown substantial improvement. Consequently, there is a pressing need to identify new tumour markers to evaluate patient prognosis and direct treatment strategies.

It has been shown that there is a close relationship between sodium overload and induction of cell necrosis [3]. Necrocide 1 (NC1) is a compound that induces necrotic cell death through sodium overload. Fo et al. [4]. identified TRPM4 as a key gene for maintaining NC1-induced cell death by screening and knocking down several genes in breast cancer. Transient receptor potential melastatin 4 (TRPM4) belongs to the TRP family and is expressed in numerous organs, with the highest expression levels observed in the prostate, colon, and heart. TRPM4 is a calcium-activated, non-selective, monovalent cation channel protein. The excessive accumulation of intracellular sodium ions it induces disrupts mitochondrial membrane potential, triggers endoplasmic reticulum stress, and initiates caspase-independent cell death mechanisms. The model which relies on NC1 triggers TRPM4 induces cell necrosis with marked sodium inward and potassium outward currents is called necrosis by sodium overload(NECSO). As a core effector molecule of NECSO, the calcium-activated sodium-selective ion channel TRPM4 plays a pivotal role in translating ionic stress into cellular responses. In recent years, TRPM4 has been found to be associated with cardiovascular diseases, neurological disorders, and immune system diseases [5]. In the field of oncology, TRPM4 contributes to several cancer hallmark functions, such as cell migration, proliferation, and the epithelial to mesenchymal transition (EMT). For instance, TRPM4 inhibitors can suppress the proliferation of colorectal cancer cells and interfere with their cell cycle transition [6]. In prostate cancer, TRPM4 promotes cancer cell survival and migration ability [7]. Chang et al. [8]. found elevated protein expression levels of TRPM4 in LUAD. Furthermore, by suppressing TRPM4 expression using siRNA technology, they observed that decreased TRPM4 levels significantly inhibited both the proliferation capacity and clone-forming ability of LUAD. cells. Additionally, suppression of TRPM4 expression reduced the invasive and migratory capabilities of tumor cells.

The tumour microenvironment(TME) and immune cells have a great impact on the outcome of tumour therapy [9, 10]. Notably, there are no validated findings to demonstrate the impact of this novel death pattern related genes on the TME, immune cell infiltration, and patient prognosis. In this article, TRPM4-related genes are screened through a database, and the selection of featured genes is performed by machine learning. TME and immune cell differential analyses were performed on the screened genes. Finally, patient prognosis was predicted, and sensitive drugs were screened. This study is the first comprehensive and systematic analysis of the effects of sodium overload on LUAD, and it is hoped that it will help us to make a more precise treatment plan and provide deeper insights into the treatment of LUAD in the future.

2 Material and method

2.1 Data source

Gene expression data were downloaded from the Gene Expression Omnibus (GEO) database of the National Center for Biotechnology Information (NCBI) (https://www.ncbi.nlm.nih.gov/geo/, ID: GSE31210). We retrieved and downloaded LUAD transcriptomi

c data with corresponding clinical information from The Cancer Genome Atlas (TCGA) database (https://portal.gdc.cancer.gov/). This LUAD cohort comprises 600 data points, including 59 standard samples and 541 tumour samples. Masked somatic mutation is also downloaded from the same database.

2.2 Identification of genes associated with TRPM4

TRPM4 is from previously published articles [5]. The correlation test was analyzed thorough Pearson correlation by setting the filter for the correlation coefficient to 0.3 and the p-value for the correlation test to 0.001. The top 50 genes with the most significant correlations were visualized. Finally, to enhance credibility and improve repeatability, the intersecting gen es were retrieved from the TCGA and GEO databases for subsequent analysis. To explore whether TRPM4-associated genes participate in shared biological processes, these candidate genes were further subjected to functional annotation and pathway analysis.

2.3 Functional enrichment analysis

The "clusterProfiler" and "enrichplot" package were used to perform functional enrichment analysis, including Gene Ontology (GO) and Kyoto Encyclopedia of Genes and Genomes (KEGG) pathway analyses, to reveal their biological roles. The similar results of the analyses were clustered, and a tree diagram was drawn.

2.4 Development and validation of a prognostic model for LUAD based on multivariate Cox regression

Univariate Cox analysis was conducted on TRPM4-related genes to identify those significantly associated with survival. LASSO logistic regression, a data analysis method utilizing L1 regularization to penalize regression coefficients, was employed to simplify the model, reduce multicollinearity, and prevent overfitting. By choosing the regularization parameter λ that minimized the criterion, coefficients were extracted from the LASSO model, and 19 candidate genes were identified using the "glmnet" package. The samples from the TCGA cohort and the GEO cohort were divided into high- and low-risk groups based on the median risk score, and these groups were then analyzed using the Kaplan-Meier (K-M) method. Clinical characteristics were collected from the sample, and age, sex, stage, and risk scores were pooled for multivariate analysis. The accuracy of the model was evaluated using ROC analysis with the R package "timeROC." Finally, a nomogram combining risk scores and clinical data was constructed, and correction curves were plotted.

Using the "survival" package, risk scores and clinical characteristics were subjected to univariate and multivariate COX regression analyses to determine independent prognostic fact.

2.5 Validation of riskscore

The predictive value of risk scores is assessed using the 'timeROC' package. The predictive value of risk scores is assessed using the "timeROC" package. The "pheatmap" package is employed to plot risk curves for different risk groups in the TCGA training dataset and the GEO testing dataset. Patients were grouped by age (older than 65 years), gender, and early or advanced clinical staging. Patients with different clinical characteristics

were grouped, and the 'survival' package was used to predict the prognosis of patients in the high and low-risk groups.

2.6 Construction of nomogram plot

The development of a nomogram was conducted using the "rms" package to facilitate the prediction of 1-, 3-, and 5-year survival probabilities for patients with LUAD based on individual characteristics. The evaluation of the model's diagnostic performance was conducted utilizing the "pROC" package.

2.7 Immunity correlation analysis

Immune cell infiltration was estimated using the CIBERSORT algorithm and analyzed across risk groups and between immune cells. We also examined the expression levels of immune checkpoints and analyzed the differences between the high-risk and low-risk groups. Spearman's correlation analysis was used to examine the relationship between immune cells and core genes. In addition, we used the ESTIMATE algorithm to assess the relationship between tumour purity and risk scores, including estimated score, immune score, and stromal score. It is essential to recognize that the tumour immune microenvironment plays a crucial role in cancer development and treatment.

2.8 Analysis of mutated landscapes

We obtained single nucleotide polymorphism (SNP) data for LUAD from the TCGA database. We used MAFTOOL software to reveal the maps of top-ranked mutated genes in the high- and low-risk groups, as well as their mutation types and mutation frequencies, and assessed the correlation between the number of mutations and risk scores. In addition, we analyzed the tumour mutational burden (TMB) in the high-risk group. tumour mutation burden for LUAD was obtained from TCGA. The tumour mutation burdens of high- and low-risk groups were compared simultaneously, and KM curves were plotted to assess the impact on patient prognosis.

2.9 Immunotherapy response and drug sensitivity

The IMvigor 210 cohort of patients receiving anti-PD-L1 therapy was used to evaluate the differences in response to immunotherapy and survival outcomes between the low-risk and high-risk groups. Subsequently, the efficacy of commonly used anticancer drugs between the two subgroups was determined based on the 50% inhibitory concentration (IC50) values obtained from the Genomics of Drug Sensitivity in Cancer database (GDSC) by the "oncopredict" package.

2.10 Characterization of by single-cell RNA sequencing

Single-cell RNA-seq data of 15 LUAD samples were obtained from GSE131907 in the GEO database. Single-cell transcriptome data were derived from GSE131907 (https://figshare.com/articles/dataset/GSE131907/19747660), and quality control standards and cell annotations were referred to the original text. Cells from lung cancer primary foci were extracted for subsequent analyses following the standard procedure of the Seurat package. The Harmony package was used to remove batch effects between samples. Parameters in the ScaleData function vars.to.regress = c("nFeature_RNA," "Percent.mt",

'CC.Difference')). The Harmony package was used to remove batch effects between samples. The remaining parameters are default values.

Spatial transcriptome data were derived from GSE189487. Subsequent analyses were performed using the Seurat package, in which Spots were normalized using SCTransform. Parameters are all default values. Cell annotation file downloaded from https://www.ncbi.nlm.nih.gov/geo/download/?acc=GSE131907.

2.11 Statistical analysis

All statistical tests and bioinformatics analyze in this study were completed by R software version 4.4.2. The p-value of less than 0.05 was considered statistically significant.

2.12 Result

2.13 Identification of TRPM4 related genes and function enrichment

LUAD data were downloaded from TCGA, and correlation tests were performed with TRPM4. A total of 169 correlated genes were derived. GO analysis revealed higher enrichment in establishment secretion extracellular region (Fig. 1A, C) (Supplement 5). The KEGG enrichment analysis showed that acid actin biosynthesis virus and Endocrine Endocytosis cycle calcium were more enriched and more significant (Fig. 1B, D) (Supplement 6). The current analysis indicates that the gene set is significantly enriched in a complex signaling network, whose core functions involve hormone regulation, cellular endocytosis mechanisms, calcium ion signaling, or a host cell network exploited by viruses. Taking the intersection in TCGA and GEO data yielded a total of 147 related genes (Supplement 1). The top 50 genes are visualized in Fig. 1E (Supplement 2). Using these top 50 genes for univariate COX regression analysis showed a significant association between 26 genes and prognosis. (Fig. 1F, Supplement 7). The HR values of ACAD8, SLC27A1, CASZ1, RPS6KA1, GLB1L2, ADCY9, PPFIBP2, and PRDM16 were less than 1, indicating that the expression of these genes reduced the prognostic risk for patients and acted as protective genes. The remaining genes are risk genes.

2.14 Development of the TIRG model and prognostic value

The LASSO regression model was constructed based on the results of the univariate COX regression analysis. Ultimately, 19 hub genes were used to construct the risk model. The risk score is calculated as follows: RiskScore = SLC52A3*0.0756686900990753 + RNPEPL1*0.100801667089581 + ACAD8* (−0.028204871) + B3GNT3*0.00153902405544514 + PLEKHA6*0.134233619186048 + AKT1S1*0.223497574355151 + ZNF408*0.0132760903940025 + PPP2R1A*0.165193570510211 + SLC27A1*(−0.174456109) + CASZ1*(−0.187574901) + LMNA*0.102997383405744 + PDXK*0.12601497598454 + CAPN15*0.0953271868856612 + RPS6KA1*(−0.095552409) + GLB1L2*(−0.00880423) + ADCY9*(−0.096627693) + PPFIBP2*(−0.033099341) + PRDM16*(−0.048212248) + AP2A1*0.0205559993668874 (Supplement 8).

The samples from the GEO and TCGA datasets were divided into high- and low-risk groups based on the mean risk score. Based on the K-M curves, it is evident that there is a significant difference between the high- and low-risk groups, with a shorter prognosis for patients in the high-risk group (Fig. 2C and D). The Progression-Free Survival (PFS) of patients in the TCGA cohort was compared according to the median risk score, and

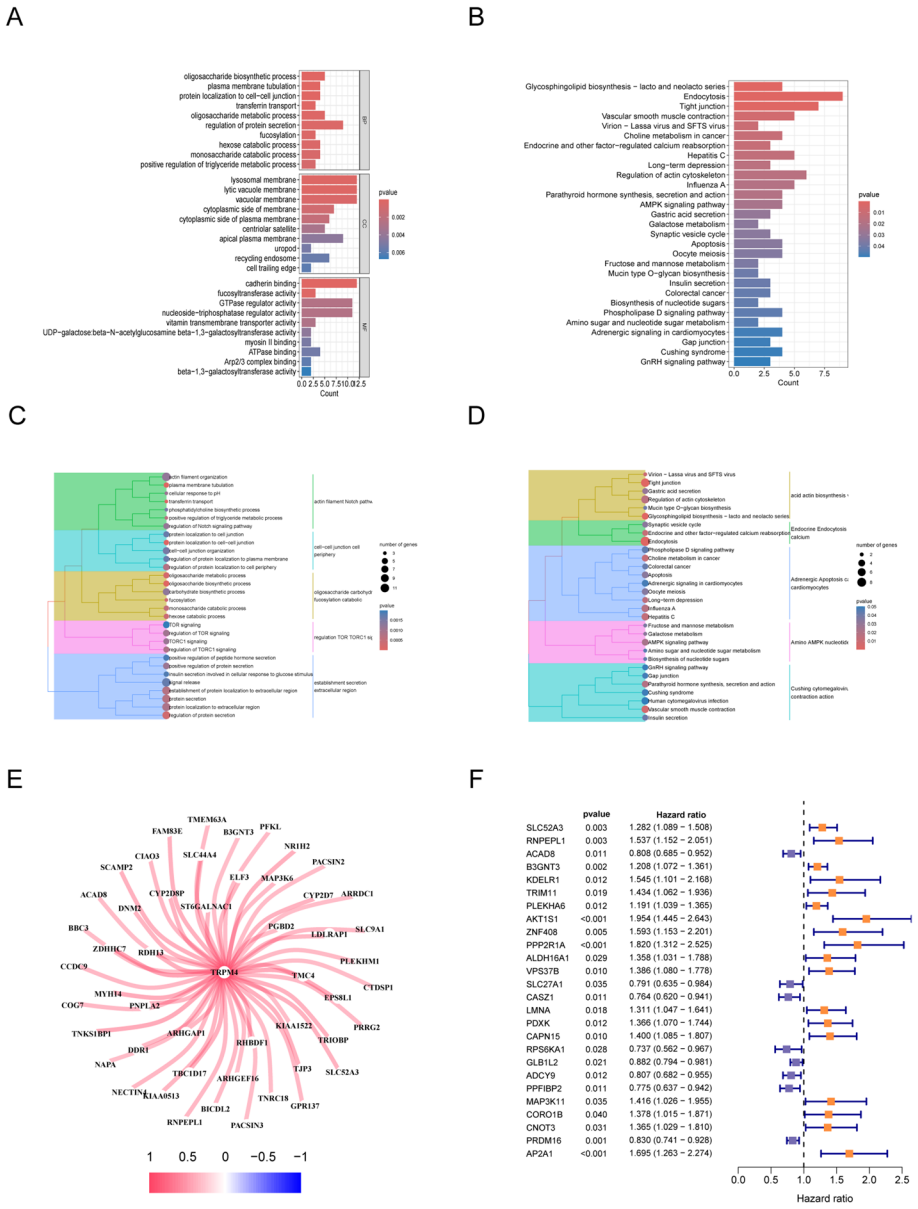

Fig. 1 The screened NRGs and function. **A** Barplot of GO enrichment analysis. **B** Barplot of Kegg enrichment analysis. **C** Treeplot of GO enrichment analysis. **D** Treeplot of Kegg enrichment analysis. **E** Co-expression network of TRPM4. **F** Forest map of prognosis-related genes

similarly, a significant difference was found between patients in the high- and low-risk groups with shorter PFS (Fig. 2E). Risk scores and clinical characteristics were included in a multifactorial analysis, and stage and risk scores were identified as prognostic influencers, with risk scores being the most significant (Fig. 2F and G).

2.15 Validation of riskscore model

By plotting the ROC curve, it was found that the scoring score had a high predictive value for patients at 1, 3, and 5 years (Fig. 3A). The clinical characteristics of the patients were re-examined, and it was found that the risk score still had a high predictive value (Fig. 3B). The distribution of patients in different risk groups in the TCGA and GEO databases, as shown in Fig. 3B and C, revealed that the prognosis of patients in the

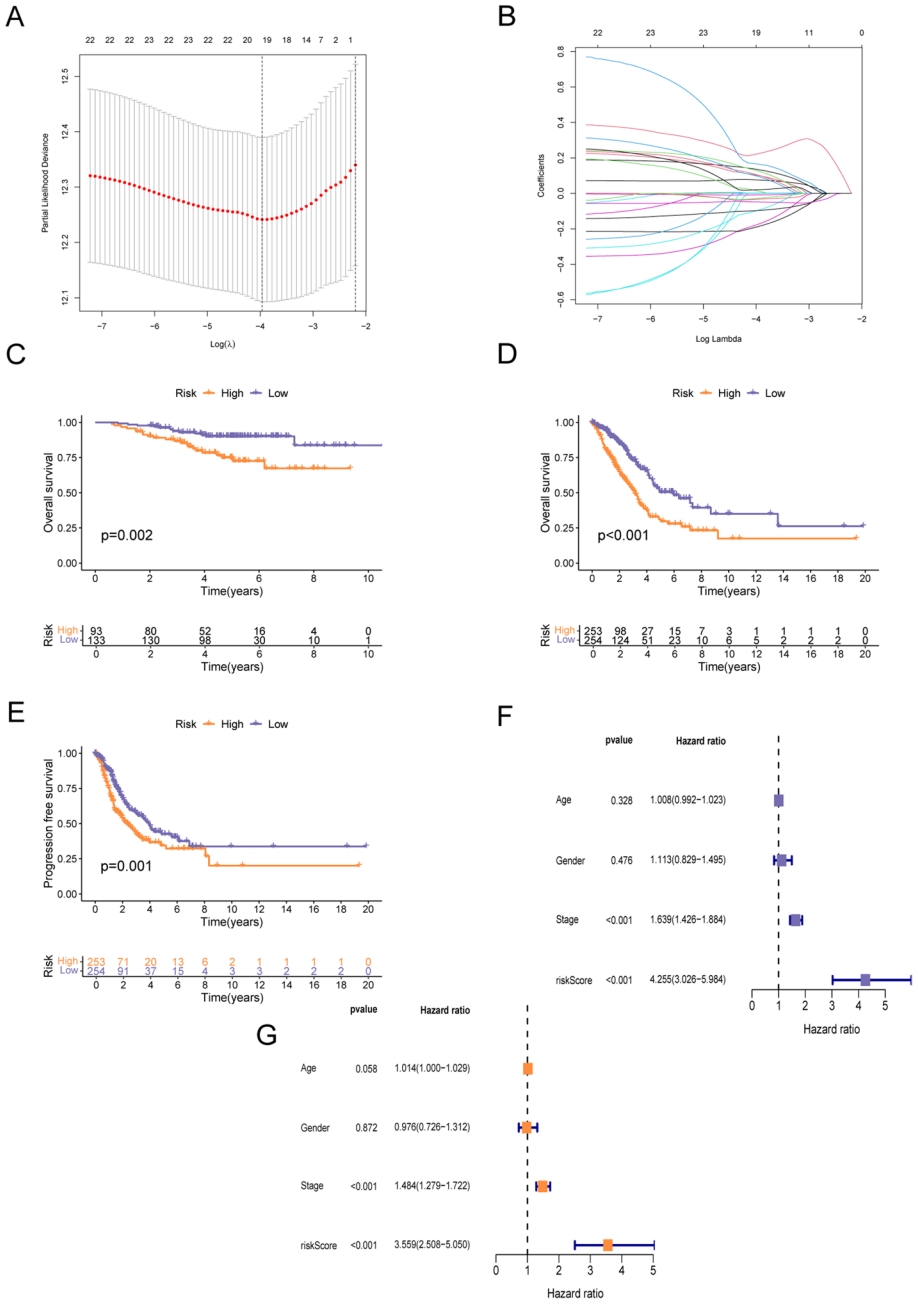

Fig. 2 Development of risk profiles in LUAD patients. **A** Cross-validation curve from LASSO regression analysis. **B** Coefcient path plot from LASSO regression analysis. **C** Differences in survival between patients in the high and low-risk groups in the TCGA database. **D** Differences in survival between patients in the high and low-risk groups in the TCGA database. **E** Differences in PFS between high and low-risk groups. **F** Results of univariate analyses of clinical characteristics and risk models. **G** Results of multivariate analyses of clinical characteristics and risk models

low-risk group was significantly better than that of patients in the high-risk group. By plotting the ROC curve, it was found that the scoring score had a high predictive value for patients at 1, 3, and 5 years. The clinical characteristics of the patients were re-examined, and it was found that the risk score still had a high predictive value. The distribution of patients in different risk groups in the TCGA and GEO databases, as shown in Fig. 3B–D, revealed that the prognosis of patients in the low-risk group was significantly better than that of patients in the high-risk group. By classifying patients with different

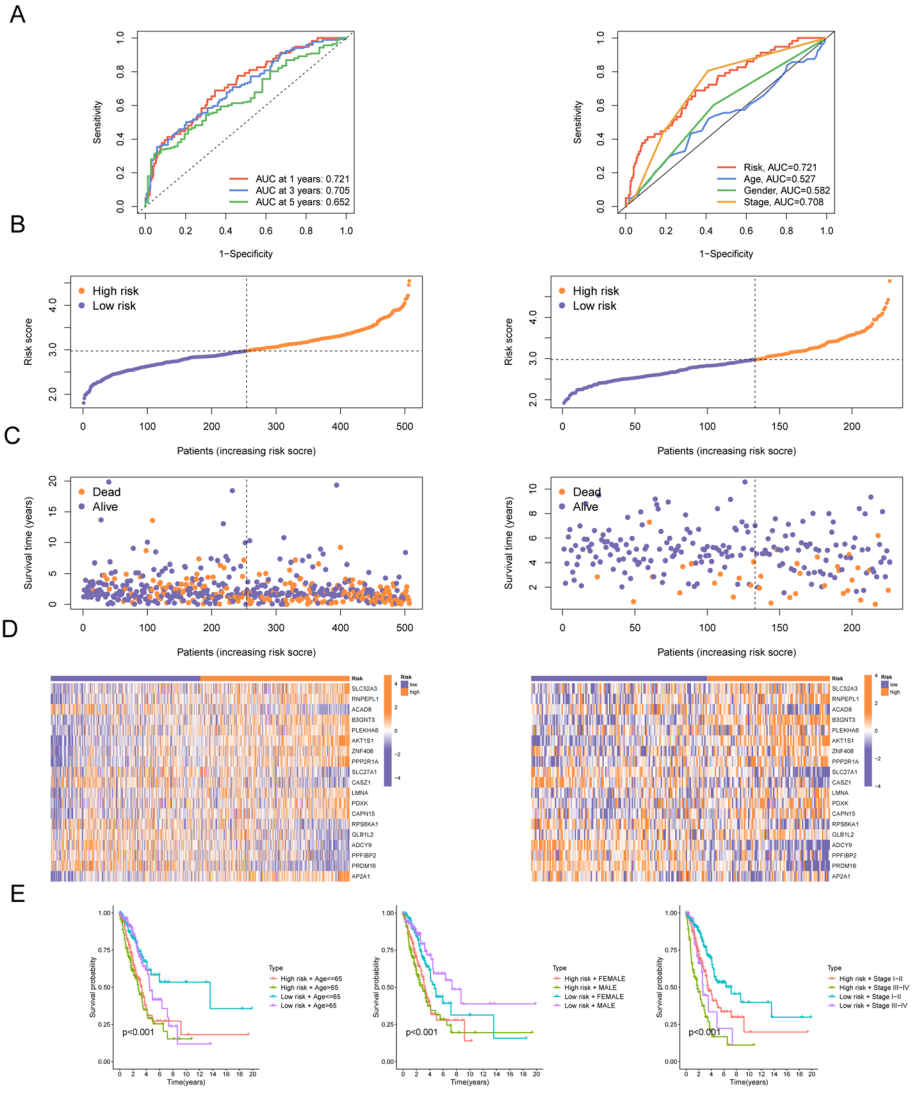

Fig. 3 Prediction of prognosis by different risk score. **A** Predictive Value of Risk Scores and Clinical Characteristics for Patient Survival at 1 Year, 3 Years, 5 Years. **B**, **C** Relationship Between Survival Status and Risk Scores in TCGA training sets and GEO testing sets. **D** Differences in gene expression between patients in different risk groups in the TCGA training sets and GEO testing sets. **E** Prognostic differences in different risk scores across clinical characteristics (age, sex, stage)

clinical characteristics, it was found that the prognosis of patients with different ages, genders, and stages was significantly different, and the prognosis of patients in the low-risk group was significantly better than that of patients in the high-risk group (Fig. 3E).

2.16 Construction of nomogram

Furthermore, a nomogram model integrating clinical features and the risk score was developed, which exhibited a high diagnostic capacity with an area under curve (AUC) value of 0.836 (Fig. 4A). The calibration curve shows that nomogram has a high predictive value (Fig. 4B).

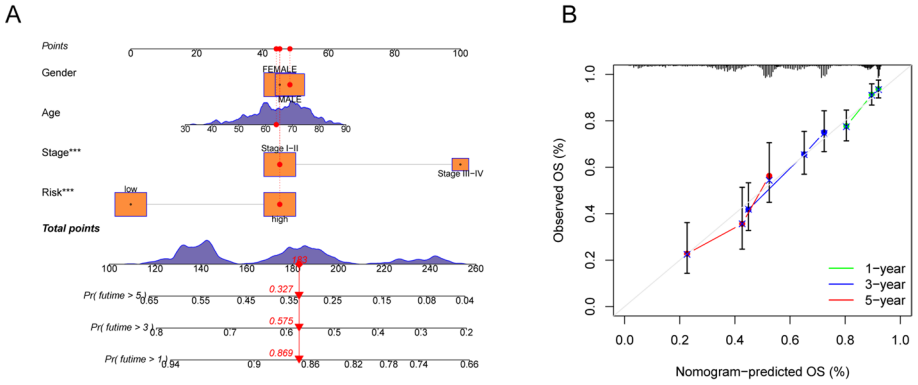

Fig. 4 construction of nomogram plot. **A** Nomogram for 1–3, and 5-years overall survival prediction. **B** Calibration plots for agreement tests between predicted and actual OS

2.17 Differences between risk subgroups and immunity

In the study, there were significant differences in immune cell infiltration between the high and low-risk groups, including the T cells CD, T cells CD4 memory resting, T cells CD4 memory activate, T cells follicular helpe, T cells regulatory (Tregs), Monocytes, Macrophages M0, Macrophages M1, Dendritic cells resting, Mast cells resting. Among them, Macrophages M0, Monocyte, T cells gamma delta, and T cells CD8 were significantly higher in the high-risk group than in the low-risk group (Fig. 5A). The relationship between core genes and immune cells was further explored (Fig. 5B). T cells are CD4 memory activated, and Plasma cells are negatively correlated with almost all core genes. Otherwise, other immune cells were positively correlated with most of the key genes. In terms of immune checkpoint expression, almost all immune checkpoints differed in expression between risk groups (Fig. 5C). In the high-risk group, TNFRSF, TNFSF, and CD276 expression were higher than in the low-risk group. At the same time, other immune checkpoints were highly expressed in the low-risk group. Tumour microenvironmental differences between the two groups were further explored. In the low-risk group, StromalScore, ImmuneScore, and ESTIMATEScore were significantly higher than in the high-risk group (Fig. 5D).

Additionally, TMB was also assessed. The low-risk group was significantly higher than the high-risk group (Fig. 5E). Combining different risk groups, K-M curves were plotted to assess the survival of patients in both groups. Survival of patients with a high tumour mutation burden was significantly better than that of the low tumour mutation burden population (Fig. 5F, G). A comparison of the mutation profiles of the high- and low-risk groups revealed that the mutation ratings of the high-risk group, including TP53, TTN, and MUC16, were significantly higher than those of the low-risk group (Fig. 5H, I).

2.18 Differences in drug sensitivity and immunotherapy response

Upon utilizing the IMvigor cohort, a dataset dedicated to immunotherapy, we identified a significant disparity in risk scores between the treatment-effective and ineffective groups. Notably, the effective group exhibited a considerably higher risk score compared to the ineffective group. Additionally, patients with high-risk scores have experienced an extension in their survival period, as depicted in Fig. 6A. Figure 6B and C illustrate the sensitivity of medications for the low- and high-risk groups, respectively.

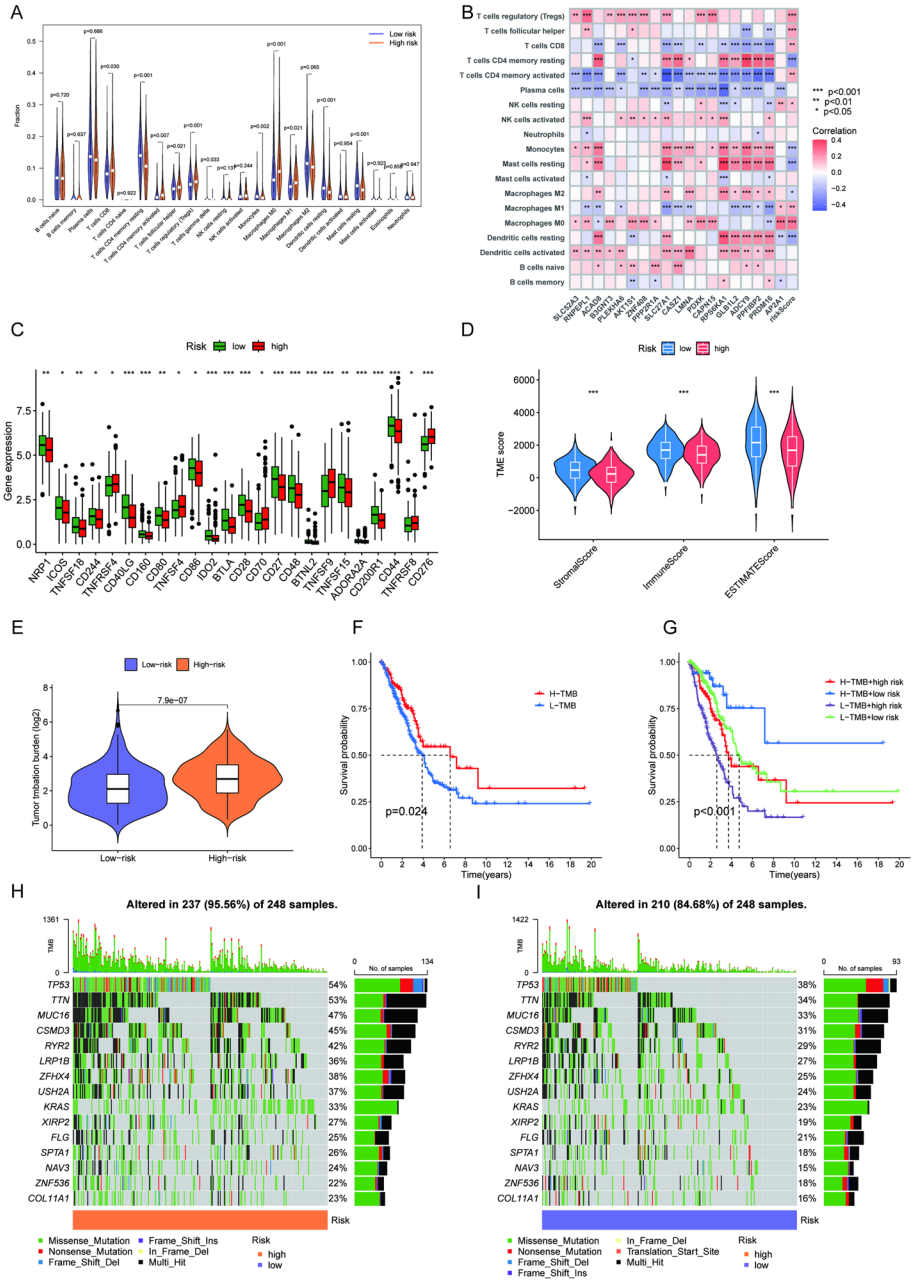

Fig. 5 Differences in immunity and gene mutation between risk subgroups. **A** Differences in immune cell infiltration between risk groups. **B** Links between immune cells and key genes. **C** Differences in expression of immune checkpoints between risk groups. **D** Differences in TME between risk groups. **E** Differences in TMB between risk groups. **F**, **G** Impact of different risk groups and TMB on patient prognosis. **H** Waterfall map displaying somatic mutations in the high-risk group. **I** Waterfall map displaying somatic mutations in the low-risk group

2.19 Overview of the scRNA-seq data generated from LUAD

We obtained single-cell sequencing data from GSE131907. The cells were annotated, as shown in Fig. 7A. In total, eight cell types were acquired (Fig. 7B). These included T cells, Endothelial cells, Mast cells, T/NK cells, Fibroblasts, Epithelial Cells, B cells, and plasma cells. To investigate the expression of marker genes in these different cells, we visualized them using Uniform Manifold Approximation and Projection (UMAP). From Fig. 7C, it was observed that TRPM4 was primarily expressed in endothelial cells and

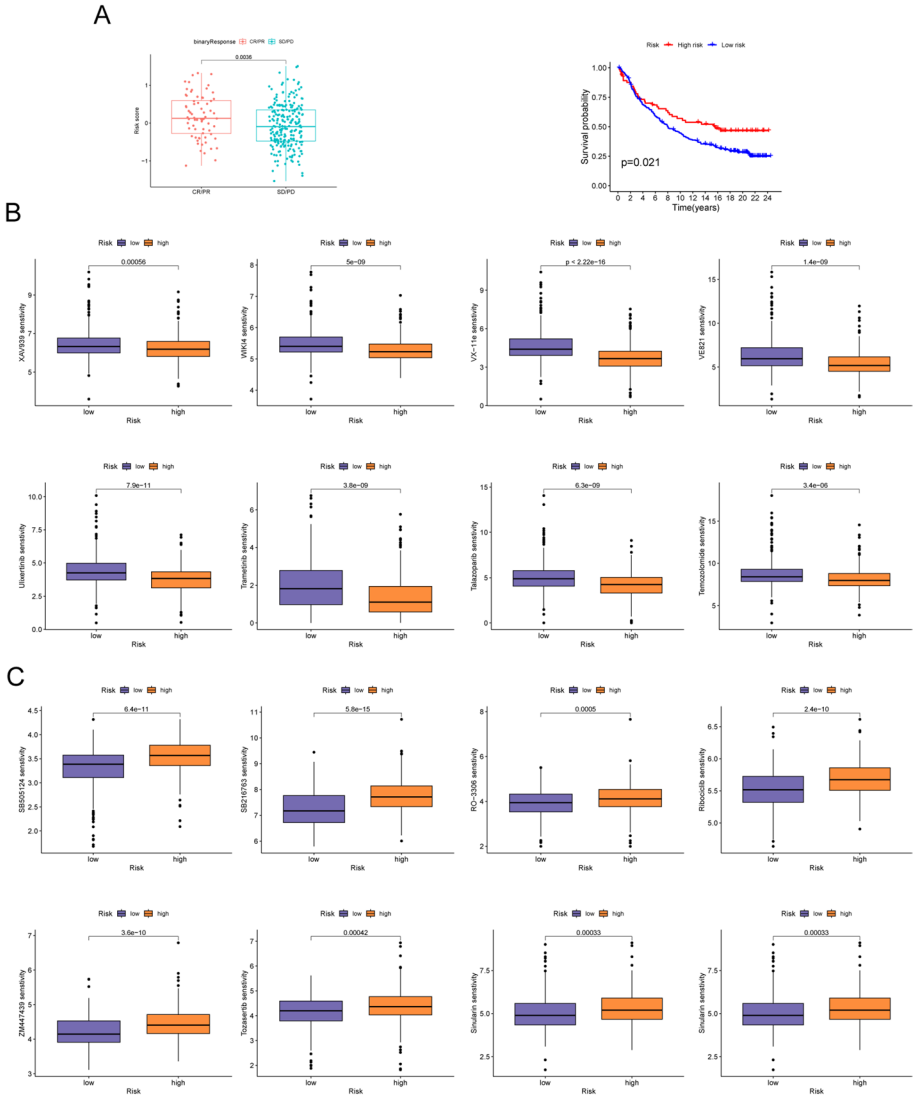

Fig. 6 **A** Violin plot comparing the risk scores between patients with different immunotherapy responses in the IMvigor cohort and K-M curves for patients with immunotherapy. **B** Box plot showing that the IC50 of drug in the low-risk group is higher than that of the high-risk group. **C** Box plot showing that the IC50 of drug in the high-risk group is higher than the low-risk group

macrophages. LMNA, PPP2R1A, PDXK, and RNPEPL1 were the most widely expressed in the TME. LMNA was predominantly expressed in endothelial cells, monocytes/macrophages, mast cells, epithelial cells, and T/NK cells. PPP2R1A was predominantly expressed in monocytes/macrophages, epithelial cells, and T/NK cells. The expression pattern of PDXK was similar to that of PPP2R1A.

2.20 Spatial transcriptome map of hub genes in LUAD

By combining spatial transcriptomics (ST) with single-cell transcriptomics (scRNA-seq) data, we constructed a comprehensive reference library. We performed stringent quality control on the data to ensure the reliability of the analyzed results. HE-stained tissues were obtained from the database for each of the three stages of LUAD development: adenocarcinoma in situ (AIS), micro invasive adenocarcinoma (MIA), and invasive adenocarcinoma cancer (IAC) (Fig. 8A, D, G). From Figure B and Figure C, it can

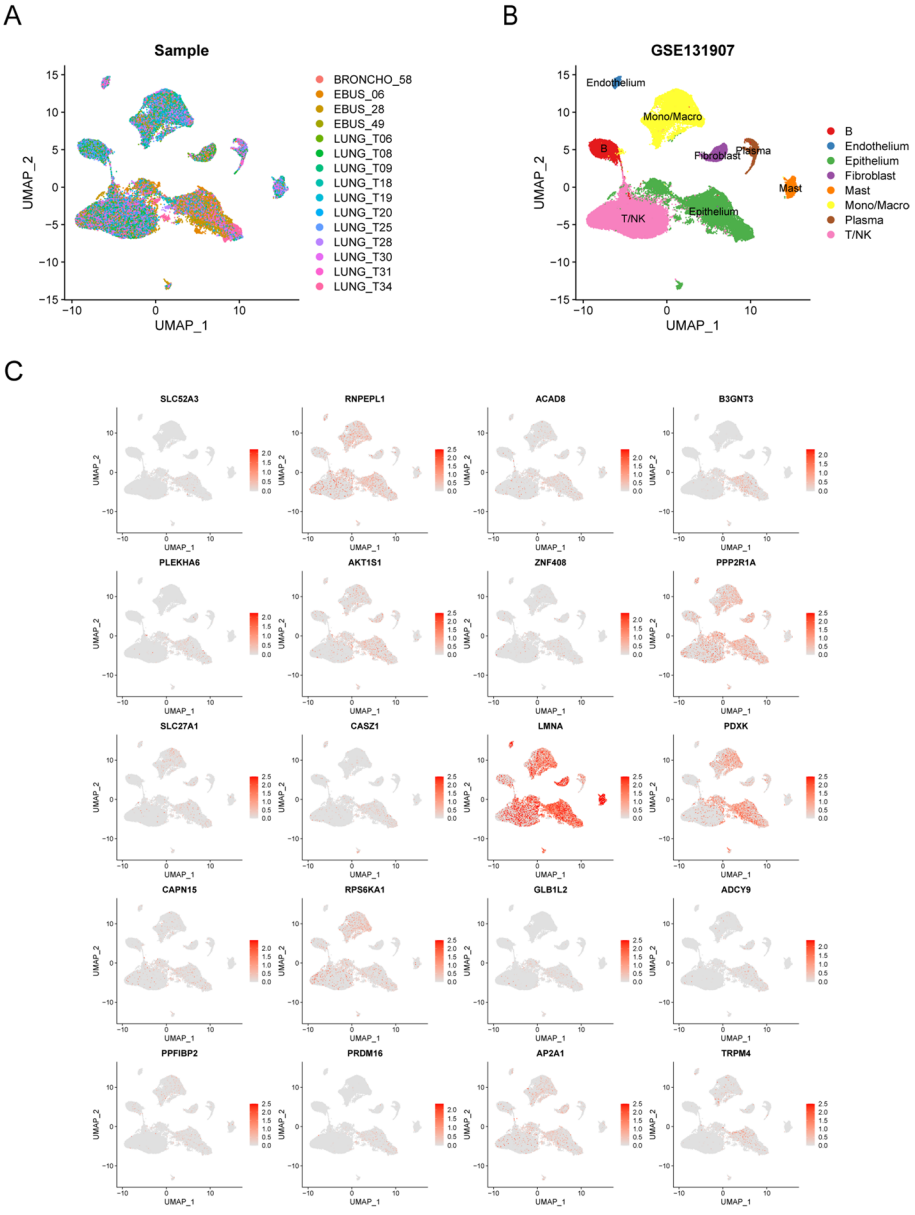

Fig. 7 Identification of hub genes through single-cell RNA sequencing analysis. **A**, **B** UMAP plots of cells generated from LUAD tissue. The plots are colored by cell cluster, and the cells are clustered into 8 sub-clusters. Each dot represents a LUAD cell. **C** The expression of signature genes in LUAD visualized in UMAP

be found that in the in AIS, LMNA, PDXK, PPP2R1A were more abundantly expressed. From Figure E and Figure F, it can be found that in the MIA, LMNA, PDXK, PPP2R1A, and RNPEPL1 were more abundantly expressed. From Figure H and Figure I, it can be noted that LMNA, PDXK, PPP2R1A, and RPS6KA1 were more abundantly expressed in the stage of IAC. Three genes, LMNA, PDXK, and PPP2R1A, were found to be more abundantly expressed with no significant changes in different stages of the same disease.

3 Discussion

Despite the rapid development of immunotherapy and targeted therapies in recent years, the overall survival of patients with LUAD has not improved as substantially as expected, and high mortality remains a major clinical challenge [10, 11]. This highlights

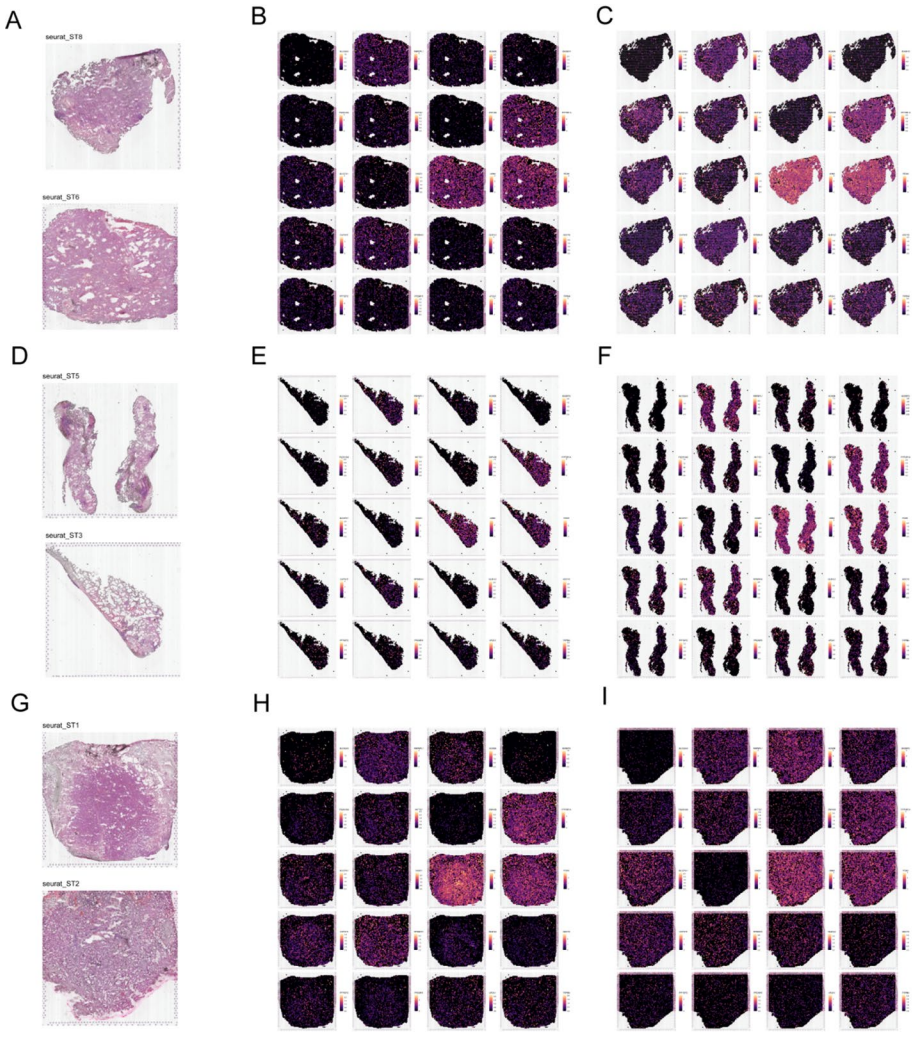

Fig. 8 Identification of hub genes through ST analysis. **A** HE-stained sections of AIS. **B**, **C** Localization of key genes in AIS. **D** HE-stained sections of MIA. **E**, **F** Localization of key genes in MIA. **G** HE-stained sections of IAC. **H**, **I** Localization of key genes in IAC

the continued need to identify novel molecular targets and regulatory mechanisms. In 2025, a newly recognized form of cell death driven by sodium-ion exchange has emerged as a potential therapeutic direction. Given the central role of immunology in cancer treatment, it is crucial to clarify whether this death modality and associated genes intersect with immune regulation in LUAD. To address this question, we screened key regulators to explore their biological functions and therapeutic relevance, focusing on TRPM4, a core gene identified in previous studies. Based on TRPM4 co-expression patterns, 169 related genes were obtained for subsequent analyses.

Our findings suggest that TRPM4-related genes may facilitate LUAD progression by influencing extracellular region secretion and endocytic pathways. These biological processes are known to regulate tumor proliferation, migration, and therapeutic resistance. For example, Wu et al. [11] demonstrated that exosomes can be internalized by EGFR-mutant LUAD cells via clathrin-dependent endocytosis, delivering wild-type EGFR and activating PI3K/AKT and MAPK pathways, thereby contributing to osimertinib resistance. Prasad et al. [12] identified HIP1, a clathrin-mediated endocytic adaptor protein,

whose depletion enhances invasiveness in NSCLC. Alterations in the extracellular region are also tightly linked to LUAD progression. Chen et al. [13] reported that miR-183-5p inhibits ECM formation and EMT in LUAD by suppressing LOXL4. Similarly, Chang et al. [14] found that ACKR2 regulates CXCL14-induced PLCβ3/PKCα/c-Src activation and promotes NF-κB–mediated EMT and migration. Altogether, these studies highlight how TRPM4-related pathways may influence LUAD biology through extracellular signaling and endocytosis.

Next, we performed LASSO regression on the TRPM4-related genes to further narrow down key markers and construct a risk-score model. This model effectively distinguished LUAD patients with significantly different prognoses and immune landscapes, demonstrating its potential value for clinical decision-making and research on the tumor microenvironment. We then integrated immune-cell profiles to explore how TRPM4-related genes correlate with immune infiltration and immunotherapy responsiveness. Notably, most immune cells showed higher infiltration in the low-risk group, indicating a more active immune microenvironment. Immune checkpoint molecules and TMB, both critical indicators for immunotherapy, also differed across risk groups. Immune checkpoint expression was higher in the low-risk group, whereas TMB showed the opposite pattern: the high-risk group exhibited higher mutational load and, correspondingly, better predicted response to immunotherapy. This is consistent with the observation that tumors with elevated TMB often generate more neoantigens and respond more favorably to immune-based treatments. In addition, mutation profiling revealed a higher frequency of TP53 alterations in the high-risk group, which may contribute to its distinct mutational characteristics. These findings collectively provide useful guidance for treatment stratification. We further evaluated drug sensitivity and found that patients in the high-risk group were more likely to benefit from immunotherapy. Meanwhile, several potentially effective therapeutic compounds were identified for different risk groups, offering additional options for personalized treatment.

We further applied single-cell sequencing and ST to examine the spatial distribution of gene expression in tumor tissues. Both analyses consistently showed that LMNA, PPP2R1A and PDXK are broadly expressed across multiple cell types and spatial regions of LUAD. These results highlight their involvement in tumor heterogeneity and support their potential relevance to immune regulation and LUAD progression. This provides a foundation for subsequent mechanistic studies and therapeutic exploration. To contextualize these observations, we reviewed existing evidence on the three genes. Although their functions in LUAD are not fully defined, studies in other cancers offer insights that support their possible involvement in tumor progression. LMNA encodes lamin proteins (types A, B and C) [15]. Prior studies reported that lamin B is highly expressed in hepatocellular carcinoma and predicts worse prognosis [16]. An altered A/C ratio may enhance nuclear deformability and promote lung cancer cell migration, while LMNA knockdown suppresses invasion through modulation of Akt/β-catenin signaling [17, 18]. PPP2R1A, a regulatory subunit of protein phosphatase 2 A, is less extensively studied. Liu et al. showed that PPP2R1A knockdown sensitizes LUAD cells to nelfinavir-induced death, whereas its overexpression increases resistance, suggesting a role in stress response and chemoresistance [19]. PDXK encodes a key enzyme in vitamin B6 metabolism. Chen et al. found that PDXK overexpression promotes migration and metastasis in hepatocellular carcinoma [20]. However, its relevance to NSCLC remains inconsistent,

with studies reporting both risk-promoting and protective associations, indicating that its precise role requires clarification [21, 23]. Together, these findings suggest that LMNA, PPP2R1A and PDXK may contribute to LUAD through mechanisms related to nuclear structure, phosphatase-mediated signaling and vitamin B6-associated metabolism. Combined with their widespread expression across tumor cell populations in single-cell and spatial analyses, these genes may influence both tumor-intrinsic biology and the tumor immune microenvironment. Although their functions in LUAD warrant further investigation, our results provide a clear rationale for prioritizing them in future mechanistic and therapeutic studies.

This study provides insights into the biological functions and clinical relevance of TRPM4-related genes in LUAD, several limitations should be acknowledged. First, all analyses were based on publicly available datasets, lacking validation in independent clinical samples; future studies should incorporate real-world cohorts to confirm the robustness of our findings. Second, although immune-microenvironment analyses suggested potential immunoregulatory roles for the identified genes, direct experimental validation in immune cells was not performed. Approaches such as immunohistochemistry, flow cytometry and CRISPR-Cas9–based functional assays will be required to clarify their mechanistic involvement in immune regulation and LUAD progression. In addition, the predictive value of drug-sensitivity patterns requires further confirmation through prospective clinical studies. Although our prognostic signature was constructed solely from TCGA and GEO cohorts, many peer-reviewed studies have successfully developed and published prognostic models based exclusively on these public datasets, indicating that such approaches can still yield meaningful and reproducible insights in a hypothesis-generating context [24]. Nevertheless, risks of overfitting and dataset-dependent gene selection remain, and all associations reported here are correlative rather than causal. Notably, the coexistence of higher TMB and specific driver-gene mutations in the high-risk group, together with differences in ESTIMATE and immune-cell infiltration patterns, likely reflects microenvironmental heterogeneity rather than a direct mechanistic contradiction [25]. The observed coexistence of high TMB and frequent TP53/TTN/MUC16 mutations in certain high-risk samples should not be overinterpreted, as the relationship between mutation burden and immune infiltration is influenced by complex microenvironmental interactions. Finally, our single-cell and spatial transcriptomic analyses serve as preliminary, hypothesis-generating assessments, relying mainly on visualization rather than fully processed pipelines. Their interpretations should therefore be cautious, and more rigorous analyses are needed to confirm cell-type specificity and spatial patterns of TRPM4-related genes in LUAD. Although there are no obvious flaws in the study design, the use of more advanced models would make the research more meaningful [26, 27].

In summary, our study identifies TRPM4-related genes as critical regulators of LUAD progression, with consistently elevated expression associated with unfavorable clinical outcomes. Their involvement in extracellular secretion and endocytic pathways underscores their potential utility as biomarkers for prognosis and predictors of therapeutic response. The spatial distribution patterns of key genes within the tumor microenvironment further support their functional relevance in LUAD development. Integrating bulk, single-cell and spatial transcriptomic evidence, we highlight LMNA, PDXK and PPP2R1A as candidate therapeutic targets with putative roles in tumor progression and

immune regulation. These findings provide a foundation for future mechanistic investigations and encourage the translation of TRPM4-based molecular insights into clinically meaningful diagnostic and therapeutic strategies for LUAD.

Supplementary Information

The online version contains supplementary material available at https://doi.org/10.1007/s12672-026-04797-5.

Supplementary Material 1.

Acknowledgements
Thanks to the researchers who provided the database data.

Author contributions
ZL M designed this study. WJ Y completed the bioinformatics analysis. WJ Y completed the writing of the manuscript. WJ Y and ZL M are co-first authors of the article. J A offered funding.

Funding
This present study was supported by "Tianshan Talents"Training Program for High level Talents in Medicine and Health of Xinjiang (No.TSYC202301B034) and State Key Laboratory of Pathogenesis, Prevention and Treatment of High Incidence Diseases in Central Asia Fund (No.SKL-HIDCA-2024-SG10).

Data availability
The datasets presented in this study can be found in online repositories. The names of the repository/repositories and accession number(s) can be found in the article/Supplementary Material.

Declarations

Ethics approval and consent to participate
Not applicable.

Consent for publication
Not applicable.

Competing interests
The authors declare no competing interests.

Received: 20 September 2025 / Accepted: 4 March 2026
Published online: 17 March 2026

References

1. Bade BC, Dela CC. Lung Cancer 2020: Epidemiology, Etiology, and Prevention. Clin Chest Med. 2020;41(1):1–24.
2. Ren J, Zhang H, Wang J, et al. Transcriptome analysis of adipocytokines and their-related LncRNAs in lung adenocarcinoma revealing the association with prognosis, immune infiltration, and metabolic characteristics. Adipocyte. 2022;11(1):250–65.
3. Ghosh S, Yang R, Duraki D, et al. Plasma Membrane Channel TRPM4 Mediates Immunogenic Therapy-Induced Necrosis. Cancer Res. 2023;83(18):3115–30.
4. Fu W, Wang J, Li T, et al. Persistent activation of TRPM4 triggers necrotic cell death characterized by sodium overload. Nat Chem Biol. 2025;21(8):1238–49.
5. Borgström A, Peinelt C, Stokłosa P. TRPM4 in Cancer-A New Potential Drug Target. Biomolecules. 2021;11(2):229.
6. Stoklosa P, Borgstrom A, Hauert B, et al. Investigation of Novel Small Molecular TRPM4 Inhibitors in Colorectal Cancer Cells. Cancers (Basel). 2021;13:21.
7. Borgstrom A, Hauert B, Kappel S, et al. Small Molecular Inhibitors Block TRPM4 Currents in Prostate Cancer Cells, with Limited Impact on Cancer Hallmark Functions. J Mol Biol. 2021;433(17):166665.
8. Chang W, Gao W, Luo B, et al. Comprehensive Insights Into the Role of TRPM4 in Pan-Cancer Progression and Immune Regulation. Immunotargets Ther. 2025;14:831–48.
9. Casey SC, Amedei A, Aquilano K, et al. Cancer prevention and therapy through the modulation of the tumor microenvironment. Semin Cancer Biol. 2015;35(SupplSuppl):S199–223.
10. Fu T, Dai LJ, Wu SY, et al. Spatial architecture of the immune microenvironment orchestrates tumor immunity and therapeutic response. J Hematol Oncol. 2021;14(1):98.
11. Wu S, Luo M, To K, et al. Intercellular transfer of exosomal wild type EGFR triggers osimertinib resistance in non-small cell lung cancer. Mol Cancer. 2021;20(1):17.
12. Prasad P, Chongtham J, Tripathi SC, et al. Targeted inhibition of NRF2 reduces the invasive and metastatic ability of HIP1 depleted lung cancer cells. Biochem Biophys Res Commun. 2024;733:150676.
13. Chen J, Zhou D, Liao H, et al. miR-183-5p regulates ECM and EMT to promote non-small cell lung cancer progression by targeting LOXL4. J Thorac Dis. 2023;15(4):1734–48.
14. Chang TM, Chiang YC, Lee CW, et al. CXCL14 promotes metastasis of non-small cell lung cancer through ACKR2-depended signaling pathway. Int J Biol Sci. 2023;19(5):1455–70.
15. Zhao J, Zhang H, Pan C, et al. Advances in research on the relationship between the LMNA gene and human diseases (Review). Mol Med Rep. 2024;30(6):236.

16. Liu H, Li D, Zhou L, et al. LMNA functions as an oncogene in hepatocellular carcinoma by regulating the proliferation and migration ability. J Cell Mol Med. 2020;24(20):12008–19.
17. Guinde J, Frankel D, Perrin S, et al. Lamins in lung cancer: biomarkers and key factors for disease progression through miR-9 regulation? Cells. 2018;7(7):78.
18. Xin H, Tang Y, Jin YH, et al. Knockdown of LMNA inhibits Akt/beta-catenin-mediated cell invasion and migration in clear cell renal cell carcinoma cells. Cell Adh Migr. 2023;17(1):1–14.
19. Liu Y, Ouyang L, Jiang S, et al. PPP2R1A silencing suppresses LUAD progression by sensitizing cells to nelfinavir-induced apoptosis and pyroptosis. Cancer Cell Int. 2024;24(1):145.
20. Chen Y, Tang L, Huang W, et al. Identification of a prognostic cuproptosis-related signature in hepatocellular carcinoma. Biol Direct. 2023;18(1):4.
21. Liu L, Yu H, Bai J, et al. Positive association of serum vitamin B6 levels with intrapulmonary lymph node and/or localized pleural metastases in non-small cell lung cancer: a retrospective study. Nutrients. 2023;15(10):2340.
22. Brasky TM, White E, Chen CL, Long-Term. Supplemental, One-Carbon Metabolism-Related Vitamin B Use in Relation to Lung Cancer Risk in the Vitamins and Lifestyle (VITAL) Cohort. J Clin Oncol. 2017;35(30):3440–8.
23. Michels J, Adam J, Goubar A, et al. Negative prognostic value of high levels of intracellular poly(ADP-ribose) in non-small cell lung cancer. Ann Oncol. 2015;26(12):2470–7.
24. Jiang F, Lin H, Yan H, et al. Construction of mRNA prognosis signature associated with differentially expressed genes in early stage of stomach adenocarcinomas based on TCGA and GEO datasets. Eur J Med Res. 2022;27(1):205.
25. Zhao X, Yan H, Yan X, et al. A novel prognostic four-gene signature of breast cancer identified by integrated bioinformatics analysis. Dis Markers. 2022;2022(1):5925982.
26. Luo J, Liu L, Venkateswaran S, et al. RPI-Bind: a structure-based method for accurate identification of RNA-protein binding sites. Sci Rep. 2017;7(1):614.
27. Song Q, Wang H, Bao J, et al. Systems biology approach to studying proliferation-dependent prognostic subnetworks in breast cancer. Sci Rep. 2015;5:12981.

Publisher's Note

Springer Nature remains neutral with regard to jurisdictional claims in published maps and institutional affiliations.